Exact and density matrix renormalization group studies of two mixed spin-$(\frac{1}{2}, \frac{5}{2}, \frac{1}{2})$ branched-chain models developed for a heterotrimetallic Fe-Mn-Cu coordination polymer

Fabiana Souza [1], Luan M. Veríssimo [1], Jozef Strečka [2], Marcelo L. Lyra [1], and Maria S. S. Pereira [1]

[1]*Instituto de Física, Universidade Federal de Alagoas, 57072-970 Maceió, Alagoas, Brazil*

[2]*Department of Theoretical Physics and Astrophysics, Faculty of Science, P. J. Šafárik University, Park Angelinum 9, 040 01 Košice, Slovakia*

The mixed-spin Ising-Heisenberg and Heisenberg branched chains whose magnetic backbone consists of regularly alternating spins 1/2 and 5/2, the latter of which are additionally coupled to an extra spin 1/2 providing lateral branching, are investigated using exact analytical and density matrix renormalization group (DMRG) methods. The proposed spin-chain models capture some relevant aspects of the heterotrimetallic coordination polymer $[CuMn(L)][Fe(bpb)(CN)_2] \cdot ClO_4 \cdot H_2O$. The mixed spin-(1/2, 5/2, 1/2) Ising-Heisenberg branched chain is exactly solvable under the assumption of an Ising-like exchange coupling along the chain, while the lateral branching is treated as an anisotropic XXZ Heisenberg exchange interaction. We determine the ground-state phase diagram and quantify a bipartite quantum entanglement between dimers at lateral branching. It is shown that the studied mixed-spin Ising-Heisenberg branched chain accurately fits available experimental data for temperature dependence of the magnetic susceptibility. The ground-state phase diagram of the analogous mixed spin-(1/2, 5/2, 1/2) Heisenberg branched chain is obtained within the DMRG method. The ground-state phase diagrams of the Ising-Heisenberg and its full Heisenberg counterpart are contrasted. In particular, the ground-state phase diagram of the mixed-spin Heisenberg branched chain involves a special Gaussian critical point, for which a proper finite-size scaling analysis is provided to accurately estimate its location and the correlation length critical exponent.

I. INTRODUCTION

Heterotrimetallic polymeric complexes are particularly attractive compounds from both the basic scientific and applied technological viewpoints due to their fascinating structural and physicochemical properties. The presence of two or more paramagnetic ions within the same magnetic compound with a specific spacial topology leads to interesting phenomenology associated to the emergence of ferromagnetic as well as ferrimagnetic correlations. It can also promote the formation of magnetic complexes with distinct spin structures and high transition temperatures [1–4]. The multimetallic complexes also find potential applications in devices exploring their luminescent [5,6], electrical conductivity [7], and catalytic [8,9] properties. Further, they play a relevant role in some biological processes occurring in the active sites of hydrogenase enzymes [10,11].

A slow relaxation dynamics has been observed in several low-dimensional heterometallic complexes with large spin values and magnetic anisotropy [12–15]. Such slow relaxation of the magnetization is associated with a superparamagnetic behavior [16,17]. The so-called single-chain magnets (SCMs) have shown potential applications in quantum computing, spintronics, and high-density memory devices [18–22], whereas their low-temperature properties are strongly affected by quantum fluctuations [23]. In particular, magnetic frustration, field-induced phase transitions, and quantum entanglement can emerge in distinct classes of SCMs with antiferromagnetic exchange couplings [24–27].

There are several examples of molecular-based magnets, which belong to a relatively wide class of heterobimetallic coordination polymers [28–33]. On the other hand, heterotrimetallic complexes containing three distinct paramagnetic ions are much more rare as their design usually requires a more elaborate synthesis procedure [32,34–37]. After the first trimetallic complex was obtained by Verani *et al.* [38], several groups have dedicated their efforts to develop better synthesis routes for SCMs. More recently, heterotrimetallic SCMs including rare-earth ions have appeared as interesting candidates for the design of nanomagnets due to the fact that the exchange coupling between $3d$ and $4f$ ions is frequently ferromagnetic with a large exchange anisotropy [39–44]. Another two coordination polymers $[CuMn(L)][M(bpb)(CN)_2] \cdot ClO_4 \cdot H_2O$ ($M = $ Fe or Cr) containing three distinct transition-metal spin carriers were reported by Wang *et al.* [45]. In these polymeric coordination compounds, two magnetic ions regularly alternate along the main polymeric chain, while a third magnetic ion is laterally coupled to each large spin unit [45].

Recently, an exactly solvable Ising-Heisenberg spin-chain model was introduced in order to bring insights into spin correlations and quantum entanglement in the iron-based member $[CuMn(L)][Fe(bpb)(CN)_2] \cdot ClO_4 \cdot H_2O$ of the two aforementioned heterotrimetallic coordination polymers to be further abbreviated as Fe-Mn-Cu [46]. Although all magnetic ions were considered as having spin $s = 1/2$, the gyromagnetic factors were adjusted to account for the actual magnetic

moment of each magnetic ion [47]. The model was shown to reproduce qualitatively the main features of the experimental susceptibility data [29]. However, the high-temperature Curie-law limit of the magnetic susceptibility appeared to be twice as large as the experimental one. This shortcoming was directly related to the modeling of the large spin $S = 5/2$ of Mn^{2+} ions through an effective spin $s = 1/2$ with a rescaled value of the Landé g-factor, $g = 10$.

In the present work, we advance in the theoretical modeling of the heterotrimetallic coordination polymer Fe-Mn-Cu [45] by explicitly considering the quantum nature of Mn^{2+} ions with true spin value $S = 5/2$. The respective mixed spin-(1/2, 5/2, 1/2) Ising-Heisenberg branched chain can still be exactly solvable when the exchange coupling along the polymeric chain has an Ising character and the lateral coupling has a quantum anisotropic Heisenberg nature. We unveil a rich ground-state phase diagram involving new quantum phases, which could not be previously captured when modeling the Mn^{2+} ion as an effective spin $s = 1/2$ with a rescaled gyromagnetic factor. The degree of quantum entanglement within each phase is quantified by measuring the quantum concurrence following the prescription put forward by Wooters and Hill [48,49]. The temperature dependence of the susceptibility data is shown to accurately reproduce the experimental data. Finally, we present a density matrix renormalization group (DMRG) study of the full Heisenberg counterpart model. Quantum anisotropic ferrimagnetic chains are known to exhibit a variety of ground-state phases, such as gapless Tomonaga-Luttinger spin-liquid phases, intermediate gapped magnetization plateaus, Kosterlitz-Thouless critical points at which a gapped phase ends, as well as special gapless Gaussian critical points at which two gapped phases meet [50–60]. We contrast the ground-state phase diagrams of both Ising-Heisenberg and full Heisenberg branched-chain models, which show a similar structure with the exception of emergence of spin-liquid phases in a narrow parameter region of the latter fully quantum spin model. A proper finite-size scaling analysis is employed to study a special Gaussian critical point emerging in the full Heisenberg branched-chain model.

This work is organized as follows. In Sec. II we briefly describe the magnetic structure of the Fe-Mn-Cu coordination polymer and introduce the relevant mixed-spin Ising-Heisenberg branched-chain model. In Sec. III, we discuss in detail all possible ground states of the studied model obtained from the exact diagonalization and build the ground-state phase diagram as a function of the magnetic field and the ratio between the exchange couplings when assuming isotropic and strongly anisotropic exchange interaction. In Sec. IV we investigate the quantum entanglement between the Cu^{2+}-Mn^{2+} dimeric units. A fitting of experimental susceptibility data is provided in Sec. V. DMRG calculations for the isotropic Heisenberg counterpart model are presented in Sec. VI, where both constructed ground-state phase diagrams are also contrasted and a proper finite-size scaling analysis in the vicinity of an emergent Gaussian critical point is performed. The most important scientific achievements are presented in Sec. VII together with conclusions and future outlooks. Some details of the analytical calculations are given in the Appendix.
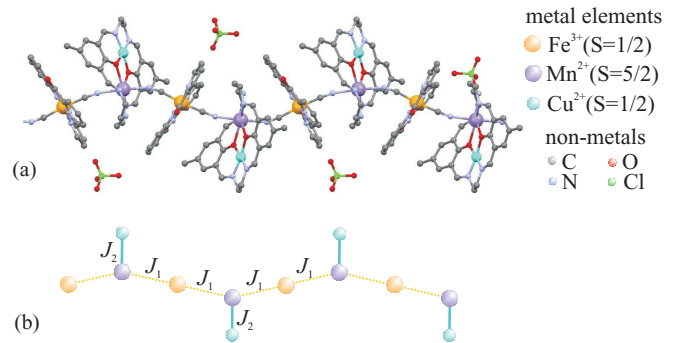
FIG. 1. (a) A part of the crystal structure of the heterotrimetallic coordination polymer $[CuMn(L)][Fe(bpb)(CN)_2] \cdot ClO_4 \cdot H_2O$ (abbreviated as Fe-Mn-Cu) visualized by adapting the crystallographic data reported in Ref. [45]. (b) A schematic illustration of the magnetic structure of the polymeric compound Fe-Mn-Cu involving two different exchange pathways between transition-metal ions, more specifically, the exchange coupling J_1 between Fe^{3+} and Mn^{2+} magnetic ions mediated by a cyanide bridge and the exchange coupling J_2 between Mn^{2+} and Cu^{2+} magnetic ions mediated by a phenolate bridge.

II. BRANCHED-CHAIN COORDINATION POLYMER AND ISING-HEISENBERG MODEL

First, let us bring insight into a magnetic structure of the heterotrimetallic coordination polymer Fe-Mn-Cu [45], the crystal structure of which is schematically depicted in Fig. 1(a). It is quite obvious from this figure that the magnetic backbone of the polymeric compound Fe-Mn-Cu constitutes a regularly alternating sequence of spin-1/2 and spin-5/2 magnetic ions Fe^{3+} and Mn^{2+} exchange coupled through a cyanide bridge, whereas each spin-5/2 magnetic ion Mn^{2+} is additionally exchange-coupled via phenolate bridge to the spin-1/2 magnetic ion Cu^{2+} forming the side branching of the coordination polymer Fe-Mn-Cu as schematically illustrated in Fig. 1(b). It is noteworthy that the strong ligand field acting on the trivalent Fe^{3+} magnetic ions is responsible for a low-spin state of this transition-metal element as well as a relatively high degree of the magnetic anisotropy [61–64].

Bearing all this in mind, the magnetic behavior of the heterotrimetallic polymeric complex Fe-Mn-Cu is at first approached by a simplified mixed spin-(1/2, 5/2, 1/2) Ising-Heisenberg branched chain, in which the exchange coupling J_1 between Fe^{3+} and Mn^{2+} magnetic ions will be assumed as an Ising-like interaction due to a relatively strong magnetic anisotropy of the low-spin magnetic ions Fe^{3+} in opposite to the exchange coupling J_2 between Mn^{2+} and Cu^{2+} magnetic ions being considered as a more general XXZ Heisenberg interaction. The Hamiltonian of the mixed spin-(1/2, 5/2, 1/2) Ising-Heisenberg branched chain can be written in this symmetric form:

$$\mathcal{H} = -J_1 \sum_{i=1}^{N_c} S_{i,1}^z (\sigma_i^z + \sigma_{i+1}^z) - J_2 \sum_{i=1}^{N_c} (\vec{S}_{i,1} \cdot \vec{S}_{i,2})_\Delta$$
$$- g\mu_B h \sum_{i=1}^{N_c} (\sigma_i^z + S_{i,1}^z + S_{i,2}^z), \quad (1)$$

TABLE I. Eigenvectors and eigenenergies (per unit cell) of all available ground states of the mixed spin-(1/2, 5/2, 1/2) Ising-Heisenberg branched chain. Notation for the classical phases: Saturated paramagnetic phase (SPA) and saturated ferrimagnetic phase (SFI). Notation for the quantum phases: Quantum unsaturated paramagnetic phase 2 (UPA-2), quantum unsaturated paramagnetic phase 1 (UPA-1), quantum unsaturated paramagnetic phase 0 (UPA-0), quantum unsaturated ferrimagnetic 2 phase (UFI-2), quantum unsaturated ferrimagnetic 1 phase (UFI-1). The probability amplitudes $a_\pm$, $c_\pm$, and $e_\pm$ are given in the main text by Eqs. (2)–(4). The total S_z of each eigenvector per unit cell is also given.

Eigenvectors $\left(\prod_i \lvert S_{i,1}, S_{i,2}\rangle \otimes \lvert\sigma_i\rangle\right)$	Eigenenergies (per unit cell)	S_z per unit cell
$\lvert\text{SPA}\rangle = \prod_i \lvert\frac{5}{2}, \frac{1}{2}\rangle_i \otimes \lvert\uparrow\rangle_i$	$E_{\text{SPA}} = -\frac{7}{2}h + \frac{5}{4} - \frac{5}{2}J_1$	$7/2$
$\lvert\text{SFI}\rangle = \prod_i \lvert\frac{5}{2}, \frac{1}{2}\rangle_i \otimes \lvert\downarrow\rangle_i$	$E_{\text{SFI}} = -\frac{5}{2}h + \frac{5}{4} + \frac{5}{2}J_1$	$5/2$
$\lvert\text{UPA-2}\rangle = \prod_i \left[a_- \lvert\frac{5}{2}, -\frac{1}{2}\rangle + a_+ \lvert\frac{3}{2}, \frac{1}{2}\rangle\right]_i \otimes \lvert\uparrow\rangle_i$	$E_{\text{UPA-2}} = -\frac{5}{2}h - \frac{1}{4} - 2J_1 - \frac{1}{2}\sqrt{(2+J_1)^2 + 5\Delta^2}$	$5/2$
$\lvert\text{UFI-2}\rangle = \prod_i \left[a_- \lvert\frac{5}{2}, -\frac{1}{2}\rangle + a_+ \lvert\frac{3}{2}, \frac{1}{2}\rangle\right]_i \otimes \lvert\downarrow\rangle_i$	$E_{\text{UFI-2}} = -\frac{3}{2}h - \frac{1}{4} + 2J_1 - \frac{1}{2}\sqrt{(2-J_1)^2 + 5\Delta^2}$	$3/2$
$\lvert\text{UPA-1}\rangle = \prod_i \left[c_- \lvert\frac{3}{2}, -\frac{1}{2}\rangle + c_+ \lvert\frac{1}{2}, \frac{1}{2}\rangle\right]_i \otimes \lvert\uparrow\rangle_i$	$E_{\text{UPA-1}} = -\frac{3}{2}h - \frac{1}{4} - J_1 - \frac{1}{2}\sqrt{(1+J_1)^2 + 8\Delta^2}$	$3/2$
$\lvert\text{UFI-1}\rangle = \prod_i \left[c_- \lvert\frac{3}{2}, -\frac{1}{2}\rangle + c_+ \lvert\frac{1}{2}, \frac{1}{2}\rangle\right]_i \otimes \lvert\downarrow\rangle_i$	$E_{\text{UFI-1}} = -\frac{1}{2}h - \frac{1}{4} + J_1 - \frac{1}{2}\sqrt{(1-J_1)^2 + 8\Delta^2}$	$1/2$
$\lvert\text{UPA-0}\rangle = \prod_i \left[e_+ \lvert\frac{1}{2}, -\frac{1}{2}\rangle + e_- \lvert-\frac{1}{2}, \frac{1}{2}\rangle\right]_i \otimes \lvert\uparrow\rangle_i$	$E_{\text{UPA-0}} = -\frac{1}{2}h - \frac{1}{4} - \frac{1}{2}\sqrt{J_1^2 + 9\Delta^2}$	$1/2$

where $(\vec{S}_{i,1} \cdot \vec{S}_{i,2})_\Delta = \Delta(S_{i,1}^x S_{i,2}^x + S_{i,1}^y S_{i,2}^y) + S_{i,1}^z S_{i,2}^z$. The Ising spin $\sigma_i^z = \pm 1/2$ corresponds to a highly anisotropic magnetic ion Fe^{3+}, while the Heisenberg spins $\vec{S}_{i,1}$ and $\vec{S}_{i,2}$ correspond to nearly isotropic magnetic ions Mn^{2+} and Cu^{2+} with spins $S = 5/2$ and $S = 1/2$, respectively. The coupling constant J_1 denotes a strength of the Ising interaction approximating the exchange coupling between Fe^{3+} and Mn^{2+} magnetic ions, while the coupling constant J_2 determines a strength of the anisotropic Heisenberg interaction between Mn^{2+} and Cu^{2+} magnetic ions with the parameter Δ quantifying a degree of the XXZ exchange anisotropy in this lateral exchange coupling. Finally, N_c denotes the number of unit cells, h is an external magnetic field, μ_B is the Bohr magnetic moment, and all magnetic ions are assumed to have the same gyromagnetic factor g. In the following two theoretical parts, we consider for simplicity a strength of the antiferromagnetic Heisenberg coupling at lateral branching as an energy unit $J_2 = -1$ and the magnetic field is also expressed in units of $g\mu_B = 1$.

III. GROUND-STATE PHASE DIAGRAM OF ISING-HEISENBERG BRANCHED CHAIN

Hamiltonian (1) of the mixed spin-(1/2, 5/2, 1/2) Ising-Heisenberg branched chain can be expressed in terms of commuting cell Hamiltonians, which can be easily exactly diagonalized (see the Appendix for a definition of the unit-cell Hamiltonian and its respective eigenvalues and eigenvectors). Consequently, all possible ground states of the mixed-spin Ising-Heisenberg branched chain can be straightforwardly constructed as a direct product of the lowest-energy eigenstates of the cell Hamiltonians. By inspection we have identified seven ground states depending on a relative strength of the exchange couplings and magnetic field. Among them, two ground states have classical nature without any quantum entanglement between spin states of the Heisenberg dimers resembling a pair of Mn^{2+} and Cu^{2+} magnetic ions residing in each lateral branching. In these two classical ground states, the Heisenberg dimers are in a direct-product state $\lvert\frac{5}{2}, \frac{1}{2}\rangle_i$, whereas the Ising spins resembling Fe^{3+} ions from a backbone of the branched chain are aligned parallel to the Heisenberg

dimers in the classical saturated paramagnetic (SPA) state and in opposite to the Heisenberg dimers in the classical saturated ferrimagnetic (SFI) state (see Table I for an explicit form of the eigenvectors).

The eigenvectors for the other five quantum-mechanically entangled ground states are also explicitly quoted in Table I. It is noteworthy that two of them have the Heisenberg dimers in the eigenstate being composed of a quantum superposition of the basis states $\lvert\frac{5}{2}, -\frac{1}{2}\rangle_i$ and $\lvert\frac{3}{2}, \frac{1}{2}\rangle_i$ with a net spin $\tilde{S} = 2$, which is aligned with respect to the Ising spins either parallel in the ground state, referred to as an unsaturated paramagnetic 2 (UPA-2) phase, or antiparallel in the ground state, referred to as an unsaturated ferrimagnetic 2 (UFI-2) phase. The other two quantum ground states have the Heisenberg dimers in a quantum superposition of the basis states $\lvert\frac{3}{2}, -\frac{1}{2}\rangle_i$ and $\lvert\frac{1}{2}, \frac{1}{2}\rangle_i$ with a net spin $\tilde{S} = 1$, which can be also aligned with respect to the Ising spins either parallel in the ground state, called an unsaturated paramagnetic 1 (UPA-1) phase, or antiparallel in the ground state, called an unsaturated ferrimagnetic 1 (UFI-1) state. Finally, the fifth quantum ground state referred to as an unsaturated paramagnetic 0 (UPA-0) phase has the Heisenberg dimers in a singletlike quantum superposition of the basis states $\lvert\frac{1}{2}, -\frac{1}{2}\rangle_i$ and $\lvert-\frac{1}{2}, \frac{1}{2}\rangle_i$ with a net spin $\tilde{S} = 0$, whereas the Ising spins are aligned parallel to the external magnetic field. For completeness, all aforementioned quantum ground states are listed together with their respective eigenvectors and eigenenergies in Table I, while the probability amplitudes emergent in the respective eigenvectors are explicitly given by

$$a_\pm^2 = \frac{1}{2}\left[1 \mp \frac{2 + \tilde{J}_1}{\sqrt{(2 + \tilde{J}_1)^2 + 5\Delta^2}}\right], \tag{2}$$

$$c_\pm^2 = \frac{1}{2}\left[1 \mp \frac{1 + \tilde{J}_1}{\sqrt{(1 + \tilde{J}_1)^2 + 8\Delta^2}}\right], \tag{3}$$

$$e_\pm^2 = \frac{1}{2}\left[1 \mp \frac{\tilde{J}_1}{\sqrt{\tilde{J}_1^2 + 9\Delta^2}}\right]. \tag{4}$$

In the above, the parameter $\tilde{J}_1$ is defined as $\tilde{J}_1 = J_1(\sigma_i^z + \sigma_{i+1}^z) = \pm J_1$, whereas a plus (minus) sign applies
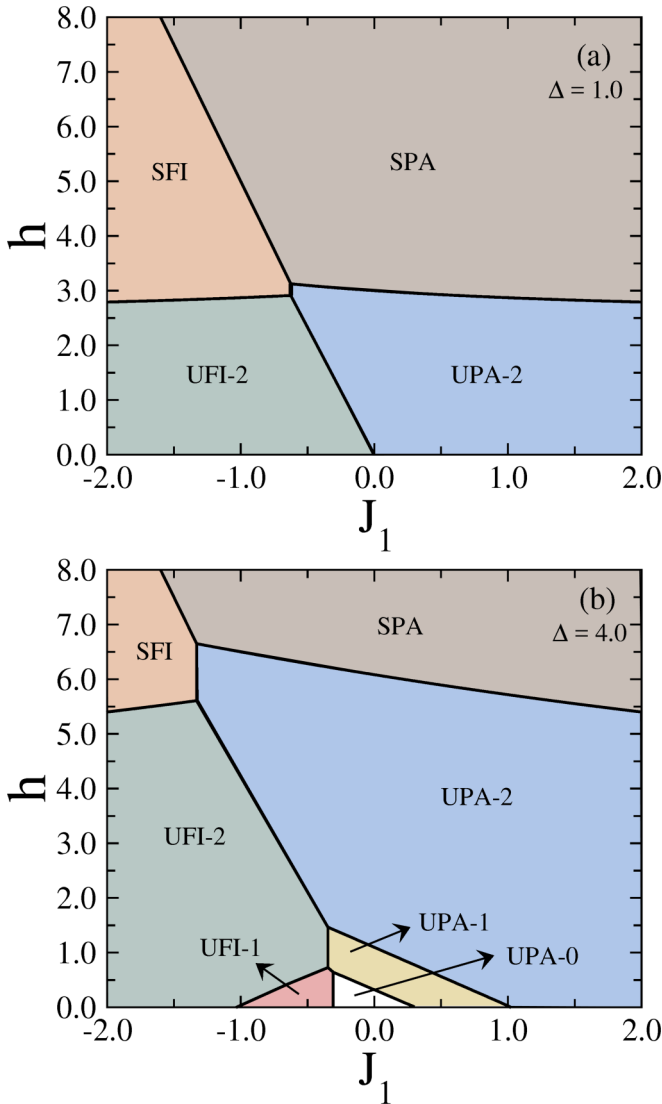
FIG. 2. Ground-state phase diagrams in the J_1-h plane for two distinct values of the anisotropy parameter: (a) $\Delta = 1.0$ and (b) $\Delta = 4.0$. The displayed phase boundaries were obtained by comparing the eigenenergies per unit cell of individual ground states as given in Table I. Note that $J_2 = -1$ and $g\mu_B = 1$ units were used.

FIG. 3. Ground-state phase diagram in the J_1-Δ plane for zero magnetic field ($h = 0$). Note that $J_2 = -1$ and $g\mu_B = 1$ units were used and the three new ground states UFI-1, UPA-0, and UPA-1 emerge just for $\Delta > 1$.

whenever the Ising spins are aligned parallel (antiparallel) with respect to the external magnetic field within the ground state with the attribute "paramagnetic" ("ferrimagnetic"). Note furthermore that the complete set of eigenvectors and eigenvalues of the cell Hamiltonian can be found in the Appendix.

The overall ground-state phase diagram is plotted in Fig. 2 in the J_1-h parameter plane for two representative values of the anisotropy parameter $\Delta = 1.0$ and 4.0 in units of $J_2 = -1.0$ and $g\mu_B = 1$. It follows from Fig. 2(a) that the ground-state phase diagram exhibits just four possible ground states for the particular case $\Delta = 1.0$ being consistent with the isotropic Heisenberg coupling. Under this condition, the classical SPA and SFI phases predominate at higher magnetic fields, while the quantum UFI-2 and UPA-2 phases prevail at lower magnetic fields. Assuming the ferromagnetic Ising

coupling constant $J_1 > 0$ one detects a single field-driven phase transition from the UPA-2 to the SPA phase upon increasing of the magnetic field. On the other hand, two different sequences of the field-induced transitions, namely, UFI-2 $\rightarrow$ UPA-2 $\rightarrow$ SPA and UFI-2 $\rightarrow$ SFI $\rightarrow$ SPA, can be detected by considering the antiferromagnetic Ising coupling constant $J_1 < 0$. The above trends are quite similar to the ones obtained previously for the purely spin-1/2 Ising-Heisenberg chain with rescaled gyromagnetic factors [46] and also hold for the Heisenberg coupling with an easy-axis exchange anisotropy $\Delta < 1$.

It should be stressed, moreover, that three new quantum phases UFI-1, UPA-1, and UPA-0 develop in the ground-state phase diagram at low enough magnetic fields when considering higher values of the anisotropy parameter $\Delta > 1$ being consistent with the Heisenberg coupling with an easy-plane exchange anisotropy [see Fig. 2(b) for $\Delta = 4.0$]. Of course, these quantum phases could not be in principle captured by modeling the Mn^{2+} ion as an effective spin-1/2 with a mere rescaled gyromagnetic factor, because stronger coupling between transverse spin components forces the Heisenberg dimers into intermediate states with lower longitudinal net spin. It could be understood from Fig. 2(b) that the additional quantum phases UFI-1, UPA-1, and UPA-0 appear in the regime of sufficiently weak Ising coupling present along the main backbone Fe^{3+}-Mn^{2+} of the polymeric chain. In this regime, a sequence of three field-driven phase transitions can be at most achieved among three quantum and one classical phase upon strengthening of the magnetic field.

Figure 3 shows the ground-state phase diagram in the J_1-Δ plane in the absence of an applied magnetic field ($h = 0$). While a direct transition between the ground states UFI-2 and UPA-2 takes place at $J_1 = 0$ for easy-axis exchange anisotropies $\Delta \leqslant 1$, three new ground states UFI-1, UPA-0,

and UPA-1 with lower net spin of the Heisenberg dimers appear for easy-plane exchange anisotropies $\Delta > 1$ on the assumption that the Ising coupling J_1 is sufficiently weak. It is worthy to note that the classical SFI and SPA phases do not represent a ground state in the zero-field limit on account of the antiferromagnetic nature of the lateral Heisenberg coupling $J_2 = -1$.

IV. QUANTUM ENTANGLEMENT

In this section, we compute the quantum concurrence for the Heisenberg dimer mimicking a pair of Mn^{2+} and Cu^{2+} magnetic ions residing in a side branching of each unit cell. This quantity serves as a measure of the quantum entanglement at zero temperature. The quantum concurrence has been widely used to quantify a quantum entanglement between two qubits, because it is a monotonous function of the entanglement of formation. As such, it vanishes for separable states formed by a direct product of the spin states of each qubit, while it becomes nonzero for nonseparable (entangled) states whereas a maximum unitary value is reached just for four Bell states.

Although the Mn^{2+} ion does not represent a single qubit with regard to its large spin value $S = 5/2$, it is of fundamental importance that only two spin components of the Mn^{2+} ion do contribute to each quantum ground state (see Table I). From this point of view, the Mn^{2+} ion with the spin $S = 5/2$ can be actually treated at zero temperature within each ground state as a qubit belonging to a two-dimensional Hilbert subspace. In what follows, we associate the state $|+\rangle$ to the state with larger z-spin projection and the state $|-\rangle$ to that with the smaller z-spin projection for each two-dimensional Hilbert subspace. In those Hilbert subspaces one may readily introduce for the originally spin-5/2 Mn^{2+} ion spin operators $\tilde{S}_1^z$, $\tilde{S}_1^x$, and $\tilde{S}_1^y$ of an effective spin qubit. The quantum concurrence can be consequently written in terms of pair spin-spin correlation functions when following the prescription established by Wooters and Hill [48,49]:

$$\mathcal{C} = \max\left\{0, 4|\langle \tilde{S}_{i,1}^x S_{i,2}^x \rangle|\right.$$
$$\left. - 2\sqrt{\left(\tfrac{1}{4} + \langle \tilde{S}_{i,1}^z S_{i,2}^z \rangle\right)^2 - \left(\tfrac{1}{2}\langle \tilde{S}_{i,1}^z + S_{i,2}^z \rangle\right)^2}\right\}, \quad (5)$$

where $\langle \tilde{S}_{i,1}^j S_{i,2}^j \rangle$ ($j = x, y, z$) are the pair spin-spin correlation functions along three orthogonal spatial directions. Owing to the XXZ symmetry of the Heisenberg coupling J_2, both transverse correlation functions are equal to each other [65], i.e., $\langle \tilde{S}_{i,1}^x S_{i,2}^x \rangle = \langle \tilde{S}_{i,1}^y S_{i,2}^y \rangle$. It turns out, moreover, that the total magnetization of the Heisenberg dimer vanishes within this effective two-qubit description; i.e., $\langle \tilde{S}_{i,1}^z + S_{i,2}^z \rangle = 0$ holds for all aforementioned quantum ground states. After some straightforward algebra, the quantum concurrence can be exactly computed from two orthogonal components of the pair spin-spin correlation function depending on a relative strength of the exchange couplings and a degree of the exchange anisotropy as it is summarized in Table II.

The quantum concurrence is depicted in Fig. 4 against the Ising exchange coupling J_1 at zero magnetic field $h = 0$ and zero temperature $T = 0$ for the same representa-

TABLE II. Quantum concurrence in the five entangled ground states UPA-0, UPA-1, UPA-2, UFI-1, and UFI-2.

Quantum phase	Quantum concurrence
UPA-0	$\mathcal{C}_{\text{UPA-0}} = \max\left\{0, \left\|\frac{3\Delta}{\sqrt{J_1^2 + 9\Delta^2}}\right\|\right\}$
UPA-1	$\mathcal{C}_{\text{UPA-1}} = \max\left\{0, \left\|\frac{2\sqrt{2}\Delta}{\sqrt{(1+J_1)^2 + 8\Delta^2}}\right\|\right\}$
UPA-2	$\mathcal{C}_{\text{UPA-2}} = \max\left\{0, \left\|\frac{\sqrt{5}\Delta}{\sqrt{(2+J_1)^2 + 5\Delta^2}}\right\|\right\}$
UFI-1	$\mathcal{C}_{\text{UFI-1}} = \max\left\{0, \left\|\frac{2\sqrt{2}\Delta}{\sqrt{(1-J_1)^2 + 8\Delta^2}}\right\|\right\}$
UFI-2	$\mathcal{C}_{\text{UFI-2}} = \max\left\{0, \left\|\frac{\sqrt{5}\Delta}{\sqrt{(2-J_1)^2 + 5\Delta^2}}\right\|\right\}$
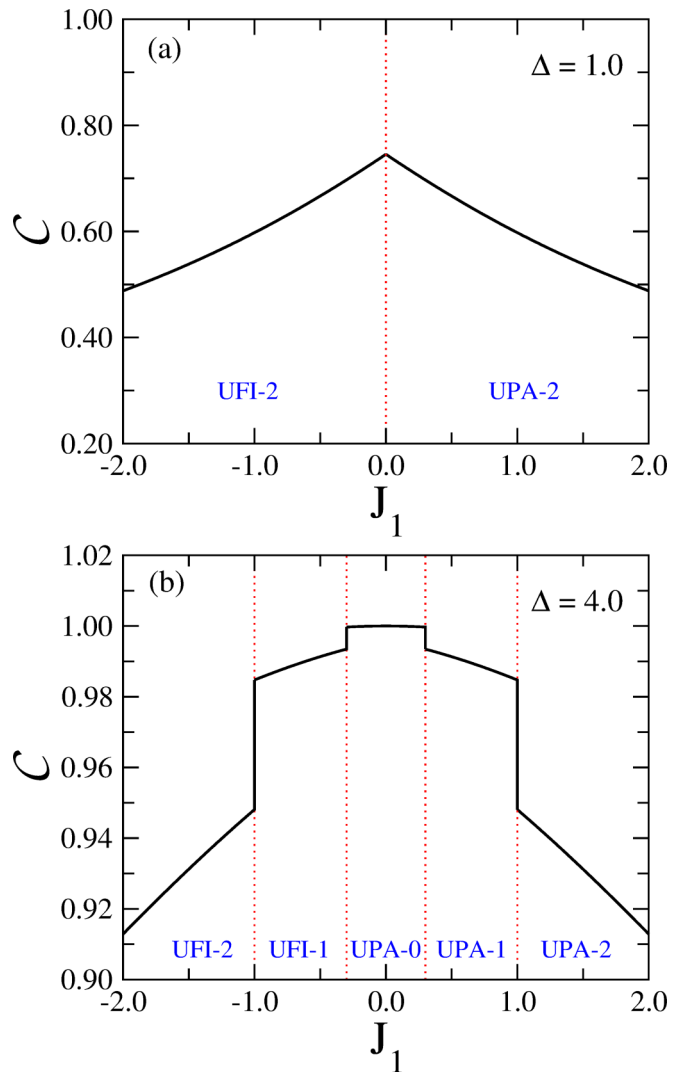
FIG. 4. The quantum concurrence of the Heisenberg dimer Mn^{2+}-Cu^{2+} as a function of the Ising exchange coupling J_1 between Fe^{3+} and Mn^{2+} magnetic ions at zero magnetic field and temperature. Abrupt jumps in the quantum concurrence illustrate possible sequences of zero-temperature phase transitions: (a) UFI-2 → UPA-2 for $\Delta = 1.0$ and (b) UFI-2 → UFI-1 → UPA-0 → UPA-1 → UPA-2 for $\Delta = 4.0$.

tive values of the exchange anisotropy as used previously. The maximum entanglement for the isotropic case $\Delta = 1.0$ shown in Fig. 4(a) is achieved for $J_1 = 0$, i.e., for a set of decoupled Heisenberg dimers Mn^{2+}-Cu^{2+}. When the Ising coupling J_1 between the Fe^{3+} and Mn^{2+} magnetic ions along the backbone of the branched chain is turned on, it suppresses a degree of quantum entanglement between the Heisenberg dimers Mn^{2+}-Cu^{2+} regardless of whether the Ising coupling between the Fe^{3+} and Mn^{2+} magnetic ions is ferromagnetic or antiferromagnetic in character. The quantum concurrence consequently displays a kink singularity at $J_1 = 0$. The quantum concurrence for a strongly anisotropic Heisenberg coupling with the exchange anisotropy $\Delta = 4.0$ is depicted in Fig. 4(b) as a function of the Ising exchange coupling J_1. An enhancement of the transverse part of the XXZ Heisenberg coupling reinforces a quantum entanglement and, hence, the quantum concurrence becomes larger within UFI-1, UPA-0, and UPA-1 ground states emergent in the regime of weak Ising coupling between the Fe^{3+} and Mn^{2+} magnetic ions. In addition, the quantum concurrence depicts jump singularities at zero-temperature phase transitions between individual ground states. It is worthwhile to remark, moreover, that the UPA-0 ground state reaches the maximum entanglement $\mathcal{C} = 1$ in the Bell form at $J_1 = 0$. It is quite clear from Fig. 4(b) that the degree of quantum entanglement remains within the UPA-0 ground state almost independent of the Ising coupling constant J_1 due to a strong transverse correlation present within the Mn^{2+}-Cu^{2+} dimer.

V. MAGNETIC SUSCEPTIBILITY

To investigate the magnetostructural properties of one-dimensional molecular-based magnetic compounds, Fegy *et al.* [66] synthesized four linear complexes where transition-metal ions Mn^{2+} regularly alternate with organic spin carriers. The magnetic behavior of one of the prepared molecular-based compounds can be described by the Heisenberg chain with regularly alternating spins $5/2$ and $1/2$ pertinent to Mn^{2+} ions and nitroxide radicals, whereas an additional nitroxide radical is laterally attached to each Mn^{2+} ion [67,68]. From this perspective, this molecular-based compound has a similar magnetic structure as the presently investigated coordination polymer Fe-Mn-Cu. In the previous studies, the transition-metal ions Mn^{2+} were considered as carrying a classical (vector) spin of size $S_j = 5/2$, while the nitroxide radicals present either along the main chain or lateral branching were assumed as quantum spins $s_i = 1/2$ with two discrete projections towards the quantization axis. Under this assumption, the linear-response theory was employed in order to calculate the magnetic susceptibility [66]:

$$\chi = \frac{g^2 \mu_B^2}{3kT} \left[S^2 + s(s+1) + s'(s'+1) - St \right. $$

$$+ \frac{1}{1-d}(-4SL + 2L^2 + 2Lt)$$

$$\left. + \frac{d}{1-d}\left(2S^2 - 2St + \frac{t^2}{2}\right) \right], \tag{6}$$

where

$$d = \frac{a_1}{3a_0}, \quad L = \frac{b_1}{3a_0} + \frac{b_0}{a_0}, \quad t = \tanh\left(\frac{x_2}{2}\right),$$

$$a_0 = 4x_1^{-2}(x_1 \sinh x_1 - \cosh x_1 + 1),$$

$$a_1 = 12x_1^{-4}\left[(x_1^3 + 12x_1)\sinh x_1 \right.$$

$$\left. - 5(x_1^2 + 12)\cosh x_1 - x_1^2 + 12\right], \tag{7}$$

$$b_0 = x_1^{-1}(\cosh x_1 - 1),$$

$$b_1 = 3x_1^{-3}\left[(x_1^2 + 4)\cosh x_1 - 4x_1 \sinh x_1 + x_1^2 - 4\right],$$

$$x_1 = -\frac{2J_1 S}{kT}, \quad \text{and} \quad x_2 = -\frac{2J_2 S}{kT}.$$

In the above, the coupling constants J_1 and J_2 refer to the exchange interactions between the spin-$5/2$ Mn^{2+} ions and the spin-$1/2$ nitroxide radicals along the main chain and laterally branching, respectively.

Alternatively, the magnetic susceptibility and other thermodynamic quantities can be exactly calculated for the proposed mixed spin-$(1/2, 5/2, 1/2)$ Ising-Heisenberg branched-chain model using the standard transfer-matrix technique. The partition function of the investigated branched spin chain can be written as

$$\mathcal{Z} = \text{Tr}\,\Lambda^{N_c}, \tag{8}$$

where the elements of the transfer matrix are given by $\Lambda_{\sigma_i \sigma_{i+1}} = \langle \sigma_i | \Lambda | \sigma_{i+1} \rangle = \sum_{j=1}^{12} e^{-\beta E_{ij}(\sigma_i, \sigma_{i+1})}$ with E_{ij} denoting the jth eigenvalue of the ith cell Hamiltonian (see Appendix) and $\beta = 1/k_B T$. In the thermodynamic limit $N_c \to \infty$, the largest eigenvalue of the transfer matrix fully determines the partition function $\mathcal{Z} = \lambda_+^{N_c}$ with

$$\lambda_+ = [(\Lambda_{++} + \Lambda_{--}) + \sqrt{(\Lambda_{++} - \Lambda_{--})^2 + 4\Lambda_{+-}^2}]/2, \tag{9}$$

from which the magnetic susceptibility and other thermodynamic quantities can be directly computed using standard relations of statistical mechanics. In particular, the total magnetization per unit cell is given by $M = k_B T \partial \ln \mathcal{Z}/\partial h$, while the zero-field magnetic susceptibility then follows from $\chi = \partial M/\partial h|_{h=0} = k_B T \partial^2 \ln \mathcal{Z}/\partial^2 h|_{h=0}$.

The available experimental data for the temperature dependence of the susceptibility times temperature product of the coordination polymer Fe-Mn-Cu [45] are compared in Fig. 5 with two aforedescribed modeling predictions based on the linear-response theory (6) adopted from Ref. [66] and the transfer-matrix solution of the mixed spin-$(1/2, 5/2, 1/2)$ Ising-Heisenberg branched chain proposed in the present work. The experimental data convincingly evidence a ferrimagnetic ordering of the heterotrimetallic polymeric compound Fe-Mn-Cu when the susceptibility times temperature product exhibits upon lowering temperature a gradual decline from its high-temperature asymptotic value being consistent with the magnitude of spins in the unit cell and their gyromagnetic factors $g = 2$; then it passes through a global minimum before it finally diverges at sufficiently low temperatures. It is noteworthy that two theoretical curves presented in Fig. 5 for the sake of comparison were calculated for the same fitting set of the exchange couplings, $J_1 = -1.22 \text{ cm}^{-1}$ for the exchange constant between the magnetic ions Fe^{3+} and Mn^{2+}
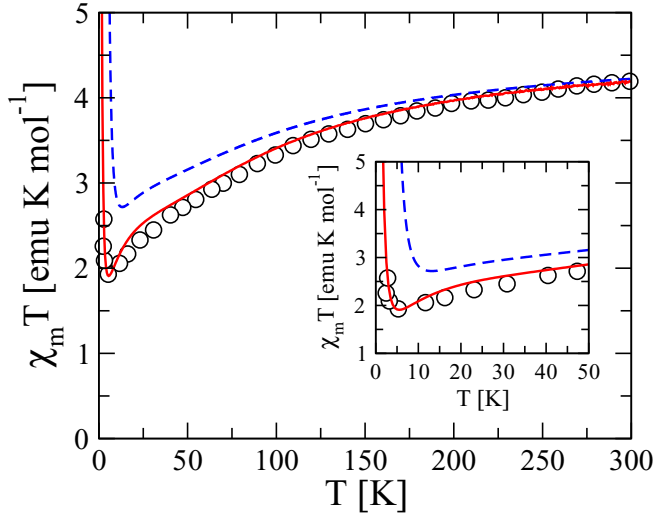
FIG. 5. Temperature dependence of χT product in units of emu K mol^{-1}. The circles represent the experimental data adapted from Ref. [29], the blue dashed line represents a theoretical prediction according to the linear-response theory adapted from Ref. [66], while the red solid line represents a theoretical prediction according to the transfer-matrix solution of the mixed spin-(1/2, 5/2, 1/2) Ising-Heisenberg branched-chain proposed in the present work using the same gyromagnetic factor $g = 2$ for all magnetic ions. Both theoretical curves are presented for the same fitting set of the exchange couplings $J_1 = -1.22$ cm^{-1} and $J_2 = -20.06$ cm^{-1} as proposed in Ref. [29] without any further adjustment. The best fit for the Ising-Heisenberg branched-chain model was obtained for the anisotropy parameter $\Delta = 1.15$, meaning that the coupling between the spin components in the XY plane ΔJ_2 is slightly larger than that between the longitudinal z components J_2.

and $J_2 = -20.06$ cm^{-1} for the exchange constant between the magnetic ions Mn^{2+} and Cu^{2+}, as estimated in the original analysis of the experimental data [45]. It is obvious from Fig. 5 that the linear-response theory developed in Ref. [66] does not properly capture the global minimum of the χT product, while the theoretical fitting based on the mixed spin-(1/2, 5/2, 1/2) Ising-Heisenberg branched-chain model fits quantitatively well the whole experimental curve including its global minimum. It should be mentioned that we have assumed without any further adjustment the same fitting set of exchange couplings as proposed in Ref. [29], whereas the best fit was obtained for $\Delta = 1.15$ as an additional fitting parameter determining a degree of the exchange anisotropy in the coupling constant between the magnetic ions Mn^{2+} and Cu^{2+}. A slightly stronger value of the coupling constant between transverse spin components of the magnetic ions Mn^{2+} and Cu^{2+} (ΔJ_2) as compared to the coupling between the longitudinal spin components (J_2) eventually compensates the fact that the Ising-like coupling between the magnetic ions Fe^{3+} and Mn^{2+} fully disregards any eventual coupling between their transverse spin components. Even so, the Ising-Heisenberg branched-chain model fits fairly well the entire experimental curve.

VI. MIXED SPIN-$(\frac{1}{2}, \frac{5}{2}, \frac{1}{2})$ HEISENBERG BRANCHED CHAIN

In this section, we consider a fully quantum mixed spin-(1/2, 5/2, 1/2) Heisenberg branched-chain model inspired by the magnetic structure of the heterotrimetallic coordination polymer Fe-Mn-Cu in order to evaluate the main differences between the ground-state phase diagrams of the mixed spin-(1/2, 5/2, 1/2) Ising-Heisenberg branched chain and its full quantum counterpart. For simplicity, our further attention will be paid only to the mixed spin-(1/2, 5/2, 1/2) Heisenberg branched chain with the perfectly isotropic exchange couplings defined through the Hamiltonian

$$\mathcal{H} = -J_1 \sum_{i=1}^{N_c} (\vec{s}_{1,i} \cdot \vec{S}_{2,i} + \vec{s}_{1,i+1} \cdot \vec{S}_{2,i}) - J_2 \sum_{i=1}^{N_c} \vec{S}_{2,i} \cdot \vec{s}_{3,i}$$

$$- g\mu_B h \sum_{i=1}^{N_c} (s_{1,i}^z + S_{2,i}^z + s_{3,i}^z), \qquad (10)$$

where the spin operators $\vec{s}_{1,i}$ correspond to the spin-1/2 Fe^{3+} magnetic ions, the spin operators $\vec{S}_{2,i}$ correspond to the spin-5/2 Mn^{2+} magnetic ions, and the spin operators $\vec{s}_{3,i}$ correspond to the laterally attached spin-1/2 Cu^{2+} magnetic ions of the polymeric compound Fe-Mn-Cu (see Fig. 1). The coupling constants J_1 and J_2 along the main chain and lateral branching are assumed to be the isotropic Heisenberg exchange couplings, h is an external magnetic field, μ_B is the Bohr magnetic moment, and g is Landé g factor. The magnetic field may play a crucial role in determining the magnetic ordering as it may induce field-driven quantum phase transitions. It should be stressed that the mixed spin-(1/2, 5/2, 1/2) Heisenberg branched-chain model is not exactly tractable and it must be therefore attacked by the state-of-the-art numerical methods such as DMRG simulations [69–71].

Numerical results

In the following, we investigate in detail the ground-state phase diagram and magnetization process of the mixed spin-(1/2, 5/2, 1/2) Heisenberg branched chain obtained upon implementation of DMRG simulations. This study will be additionally supplemented by a comprehensive finite-size scaling analysis of a special Gaussian critical point emergent in the established ground-state phase diagram. More specifically, we have performed DMRG simulations of the mixed spin-(1/2, 5/2, 1/2) Heisenberg branched chain using open-source packages from the Algorithms and Libraries for Physics Simulations (ALPS) project [72] by assuming the periodic boundary conditions and several system sizes with up to $N_c = 40$ units cells (i.e., 120 spins). Note, furthermore, that the number of kept states and the number of sweeps were adjusted in order to keep a truncation error below $\propto 10^{-9}$. Our main attention is devoted to comprehensive analysis of the ground-state phase diagram of the mixed spin-(1/2, 5/2, 1/2) Heisenberg branched chain given by Eq. (10).

Let us start our study by investigating the zero-temperature magnetization curve of the mixed spin-(1/2, 5/2, 1/2) Heisenberg branched chain by considering first the special case with both antiferromagnetic interactions of equal
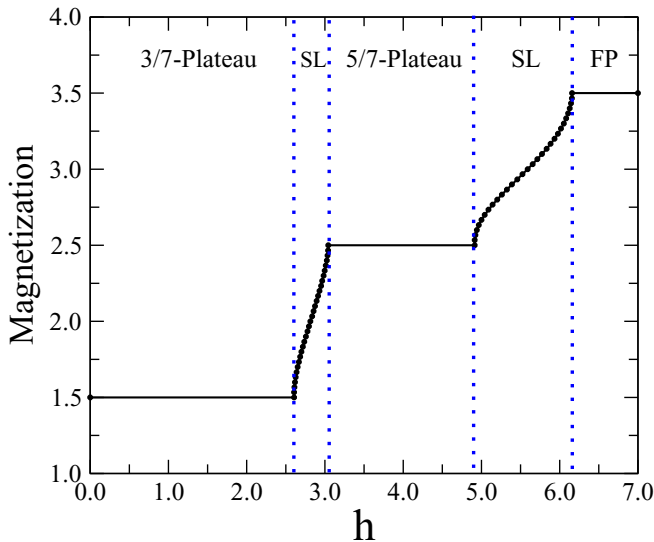
FIG. 6. The magnetization (per unit cell) curve of the mixed spin-(1/2, 5/2, 1/2) Heisenberg branched chain for the particular case with equal coupling constants $J_1 = J_2 = -1$ and $g\mu_B = 1$ units. The massive phases are represented by intermediate magnetization plateaus at 3/7 and 5/7 of the saturation magnetization, while the critical massless phase pertinent to the Tomonaga-Luttinger quantum spin liquid is characterized by a continuous rise of the magnetization with increasing of the magnetic field. All field-driven quantum phase transitions are continuous (second order). Data are from numerical calculations in chains with $N_c = 40$ unit cells and periodic boundary conditions.

strength, $J_1 = J_2 = -1$. Figure 6 shows the total magnetization normalized with respect to the saturation value as a function of the external magnetic field h. Two intermediate magnetization plateaus at 3/7 and 5/7 of the saturation magnetization can be ascribed to gapped (massive) phases with fractional values of the magnetization being consistent with the Oshikawa-Yamanaka-Affleck quantization rule [55]. The magnetization plateau at 3/7 of the saturation magnetization, which arises from zero magnetic field, can be identified according to the Lieb-Mattis theorem as the massive ferrimagnetic phase with regard to a bipartite nature of the branched spin chain [73]. The gapless critical phases, where the magnetization rises continuously upon increasing of the magnetic field, correspond to the Tomonaga-Luttinger quantum spin liquid in accordance with the massless character of the low-lying energy excitations of one-dimensional quantum spin models [74]. Note that the Tomonaga-Luttinger quantum spin liquid is wedged in between two massive phases, from which it is separated by continuous field-driven quantum phase transitions. This feature is commonly found in ferrimagnetic quantum Heisenberg spin chains [75,76]. We stress that such gapless spin liquid phases could not be captured by the Ising-Heisenberg model developed in Sec. III because the Ising nature of the coupling along the chain suppresses the quantum correlations inherent in such quantum critical phases.

Next, let us construct the ground-state phase diagram of the mixed spin-(1/2, 5/2, 1/2) Heisenberg branched chain in the J_1-h plane when using $J_2 = -1$ and $g\mu_B = 1$ units. For this

purpose, we have computed zero-temperature magnetization curves for a large series of the coupling constant J_1 along the main backbone of the branched spin chain from the interval $J_1 \in [-2, 2]$, whereas the effect of ferromagnetic ($J_1 > 0$) as well as antiferromagnetic ($J_1 < 0$) coupling constant was explored in particular. The phase boundaries between the individual ground states were obtained from DMRG results for eigenenergies $E(M, h = 0)$, which correspond to the lowest-energy eigenstates with a given total magnetization $M = \sum_{l=1}^{N_c}(s_{1,l}^z + S_{2,l}^z + s_{3,l}^z)$ in a zero magnetic field $h = 0$. The upper and lower critical fields $h^\pm$ determining a field range of the lowest-energy eigenstate belonging to the magnetization sector M are given by

$$h^+ = E(M + 1, h = 0) - E(M, h = 0),$$
$$h^- = E(M, h = 0) - E(M - 1, h = 0), \tag{11}$$

whereas the upper and lower critical fields $h^\pm$ converge to distinct values for the massive ground states being responsible for the intermediate 3/7 and 5/7 magnetization plateaus. On the other hand, the upper and lower critical fields $h^\pm$ scale in the critical (massless) ground state pertinent to the Tomonaga-Luttinger quantum spin liquid with a finite-size correction and converge in the thermodynamic limit to the following values [56,77]:

$$h^\pm \sim h(M) \pm \frac{\pi v_s \eta}{N_c}, \tag{12}$$

where $h(M)$ denotes an extrapolated value of the magnetic field producing the total magnetization M in the thermodynamic limit, v_s is the sound velocity, and η is the critical exponent for a spatial dependence of the pair correlation function [56].

The ground-state phase diagram of the mixed spin-(1/2, 5/2, 1/2) Heisenberg branched chain is depicted in Fig. 7. At low magnetic fields, one identifies two massive ground states corresponding to the intermediate magnetization plateaus. The 5/7 plateau predominates for the ferromagnetic coupling constant $J_1 > 0$, while the 3/7 plateau develops for the antiferromagnetic coupling constant $J_1 < 0$. The massive phases inherent to the 3/7 and 5/7 plateaus are separated from each other by a narrow region corresponding to the gapless quantum spin-liquid phase. Another 5/7 plateau phase can be detected at higher magnetic fields when assuming the antiferromagnetic coupling constant $J_1 < 0$. Two massive ground states with the magnetization equal to 5/7 of the saturation magnetization coalesce at a single critical point. This special critical point, at which these two gapped phases meet together, corresponds to a Gaussian critical point absent in the ground-state phase diagram of the Ising-Heisenberg counterpart model. In the regime of high magnetic fields, the gapped phase inherent to the 5/7 plateau is also separated from the fully polarized state by the Tomonaga-Luttinger quantum spin liquid. For better clarity, Fig. 7 also compares the ground-state phase diagrams of the Ising-Heisenberg and Heisenberg branched-chain models. Although the Ising-Heisenberg model is not capable of presenting a quantum spin-liquid phase, both phase diagrams exhibit quite similar features similarly as identified in the past for other quantum spin-chain models [78,79]. In fact, the upper critical field
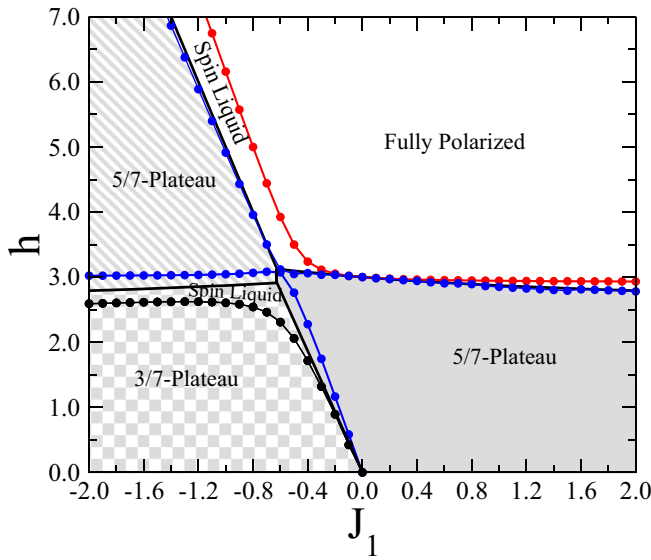
FIG. 7. A comparison between ground-state phase diagrams of the mixed spin-(1/2, 5/2, 1/2) Ising-Heisenberg branched-chain model (solid lines) and the mixed spin-(1/2, 5/2, 1/2) Heisenberg branched-chain model (solid lines with solid circles). A direct field-driven phase transition between the massive plateau phases of the Ising-Heisenberg model is replaced for the Heisenberg counterpart model by an intermediate region corresponding to the quantum spin-liquid phase. In the latter full Heisenberg model, both massive 5/7 plateau phases meet at a single Gaussian critical point. Data for the full Heisenberg model are from numerical calculations in chains with $N_c = 40$ unit cells and periodic boundary conditions.

for both 5/7 plateau phases are completely identical in both models. Further, a narrow coexistence line between two gapful 5/7 plateau phases of the Ising-Heisenberg model is replaced by a single Gaussian critical point in the full Heisenberg counterpart model.

Finally, let us focus our attention to the special critical point of the Heisenberg branched-chain model, at which two gapful 5/7 plateau phases coalesce with the gapless Tomonaga-Luttinger quantum spin liquid. This feature is characteristic for the Gaussian critical point, which appears in diverse quantum spin models [60,80–82]. To precisely locate the Gaussian critical point and determine a relevant critical exponent, we have performed a comprehensive finite-size scaling analysis of the scaled gap $\Delta_{N_c} = N_c \Delta_E$ as a function of the coupling constant J_1 for several system sizes up to $N_c = 40$ unit cells (120 spins). The scaled gap Δ_{N_c} is plotted in Fig. 8(a), where a distinct behavior can be seen as one deflects from a crossing point of four quantum-phase-transition lines determining the Gaussian critical point. Indeed, the four phase boundaries cross at the Gaussian critical point which unveils that the scaling hypothesis at this quantum critical point should obey an invariance of the scaled gap and its slope. A proper finite-size scaling hypothesis for the size dependence of the scaled gap Δ_{N_c} in the close vicinity of the Gaussian critical point can be written in the form [80]

$$\Delta_{N_c} \approx (J_1 - J_c)\alpha + f\left(\frac{\xi}{N_c}\right). \qquad (13)$$
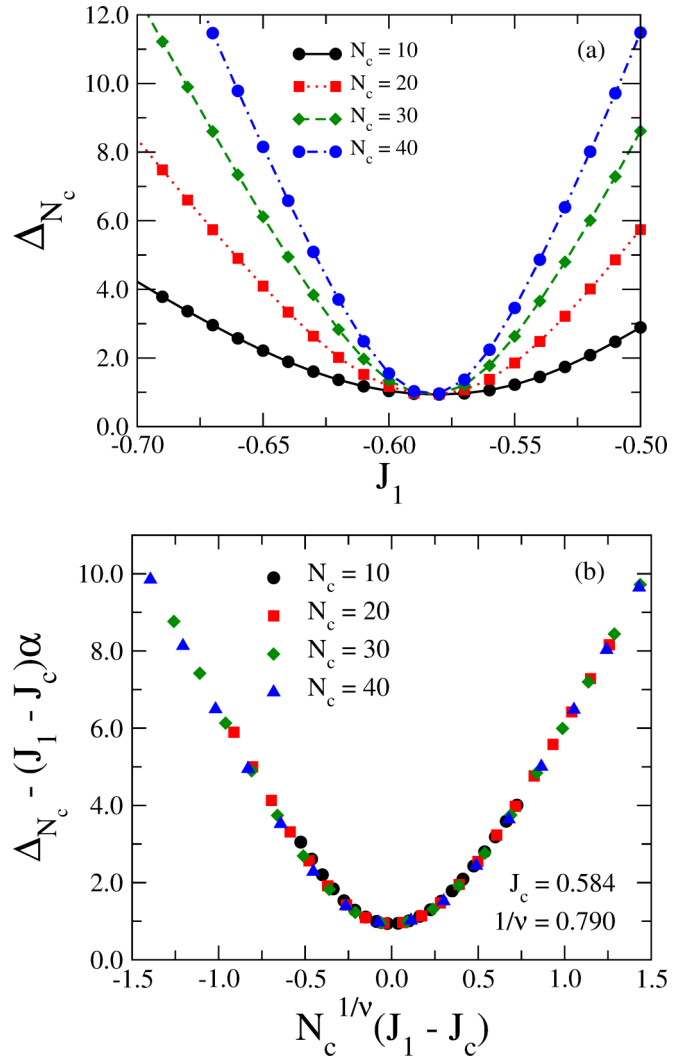
FIG. 8. (a) The scaled gap Δ_{N_c} for the magnetization sector responsible for the $\frac{5}{7}$ plateau as a function of the coupling constant J_1, which serves in evidence that the curves for the scaled gap meet together at the Gaussian critical point. (b) The data collapse of $\Delta_{N_c} - (J_1 - J_c)\alpha$ as a function of the proper scaling variable $x = N_c^{\frac{1}{\nu}}(J_1 - J_c)$, where α denotes the scale-invariant slope at the Gaussian critical point. The best data collapse provided the estimates of the critical exponent of correlation length $\frac{1}{\nu} = 0.79$, the location of the Gaussian critical point [$J_c = -0.584$; $h_c = 3.065$], and the critical slope of the scaled gap $\alpha = 1.85$.

Here, J_c is the critical value of the coupling constant J_1 and $\alpha = \Delta'_{N_c}(J_c)$ is the scale-invariant slope of phase boundaries at this quantum critical point. The correlation length ξ near the Gaussian critical point diverges as $\xi \propto |J_1 - J_c|^{-\nu}$ with ν being its characteristic critical exponent. Bearing this in mind, the scaling form (13) can be employed in order to collapse all curves into a single one and, consequently, one may get a universal curve independent of the system size when the scaled gap is plotted against $N_c^{\frac{1}{\nu}}(J_1 - J_c)$ as shown in Fig. 8(b). One actually finds that all curves coalesce into a universal one when we use our best estimate for the correlation length critical exponent $\frac{1}{\nu} = 0.79$, the locus of the Gaussian critical point $J_c = -0.584$, and the critical slope of the scaled

gap $\alpha = 1.85$. The magnetic field, at which the Gaussian critical point takes place, is estimated to be $h_c = 3.065$. Such a scaling analysis appears as an alternative protocol [80] to the twisted-boundaries technique [59] to explore critical properties of quantum spin-chain models displaying Gaussian critical points.

VII. SUMMARY AND CONCLUSIONS

In summary, two mixed spin-(1/2,5/2,1/2) branched-chain models were investigated in detail with the aim to model a ferrimagnetic behavior of the heterotrimetallic coordination polymer Fe-Mn-Cu [45]. The magnetic backbone of the polymeric compound Fe-Mn-Cu consists of regularly alternating spin-1/2 Fe^{3+} and spin-5/2 Mn^{2+} magnetic ions with an additional pendant spin-1/2 Cu^{2+} magnetic ion laterally attached to each spin-5/2 Mn^{2+} magnetic ion. The mixed spin-(1/2,5/2,1/2) Ising-Heisenberg branched chain in the presence of the magnetic field has been exactly solved by considering either ferromagnetic or antiferromagnetic Ising-type exchange coupling between Fe^{3+} and Mn^{2+} magnetic ions along the backbone of the polymeric chain, which can be justified by a relatively large anisotropy of the spin-1/2 Fe^{3+} ions in a low-spin state. Contrary to this, the more general XXZ antiferromagnetic Heisenberg exchange interaction with a single parameter Δ quantifying a degree of the exchange anisotropy was assumed between the dimeric units Mn^{2+}-Cu^{2+} being responsible for the lateral branching.

The ground-state phase diagram of the mixed spin-(1/2,5/2,1/2) Ising-Heisenberg branched-chain model may exhibit up to seven distinct phases. Two of them have a classical nature with the spins of the dimeric units Mn^{2+}-Cu^{2+} aligned parallel to the external magnetic field. The spin alignment along the main chain in these two classical ground states can be either ferromagnetic (SPA phase) or ferrimagnetic (SFI phase), depending on the relative strength of the magnetic field and the character of the Ising-type exchange coupling. The other five phases have the lateral dimers Mn^{2+}-Cu^{2+} in quantum entangled states. Two entangled ground states have the lateral dimers Mn^{2+}-Cu^{2+} in the magnetization sector with the total spin $S_T = 2$ (UPA-2 and UFI-2) and the other two ground states in the magnetization sector with the total spin $S_T = 1$ (UPA-1 and UFI-1). The remaining ground state has the lateral dimers Mn^{2+}-Cu^{2+} in the singletlike state with zero total spin $S_T = 0$ (UPA-0). It is noteworthy that the ground states with the lateral dimers Mn^{2+}-Cu^{2+} in the magnetization sectors with the total spin $S_T = 1$ and $S_T = 0$ only appear when considering the easy-plane exchange anisotropy ($\Delta > 1$) of the lateral exchange coupling J_2; i.e., the coupling between transverse spin components is stronger than that between longitudinal spin components at lateral branching.

The degree of quantum entanglement within the lateral dimeric units Mn^{2+}-Cu^{2+} was quantified by computing the quantum concurrence. It has been shown that the Ising-type coupling between Fe^{3+} and Mn^{2+} magnetic ions along the main chain gradually degrades the bipartite quantum entanglement. On the other hand, the quantum entanglement is favored by increasing the transverse part of the exchange coupling between Mn^{2+} and Cu^{2+} magnetic ions. To evalu-

ate the reliability of the present Ising-Heisenberg branched-chain model for a description of the magnetic behavior of the heterotrimetallic coordination polymer Fe-Mn-Cu, we have computed the magnetic susceptibility using the standard transfer-matrix technique. The available experimental data for the magnetic susceptibility was accurately fitted using the previous estimates of the exchange couplings [29] and an exchange anisotropy $\Delta = 1.15$.

To evaluate how the assumption of an Ising-type coupling along the main chain affects the ground-state phase diagram, we have also performed DMRG calculation for the analogous mixed spin-(1/2, 5/2, 1/2) Heisenberg branched-chain model. We have unveiled that both models present quite similar ground-state phase diagrams. The main new feature introduced by the quantum character of the exchange coupling along the backbone of the polymeric chain is the emergence of a narrow critical quantum spin-liquid phase, which separates the gapped phases pertinent to the intermediate plateaus at 3/7 and 5/7 of the saturation magnetization. Further, a narrow coexistence line between two massive ground states with the magnetization equal to 5/7 of the saturation magnetization of the Ising-Heisenberg model is replaced by a single Gaussian critical point in the respective Heisenberg model. We have performed a proper finite-size scaling analysis, which accounts for the scale invariance of the scaled gap and its derivative at the Gaussian critical point, to precisely locate this special quantum critical point and to estimate its corresponding correlation length critical exponent.

The present results support the reliability of using effective exactly solvable Ising-Heisenberg spin-chain models for a description of certain heterometallic coordination compounds. These can give a qualitative description of the ground-state phase diagram as well as accurately capture temperature dependencies of relevant thermodynamic quantities. However, one should bear in mind that some specific features can only be captured by the full Heisenberg description, such as the presence of a narrow critical Tomonago-Luttinger quantum spin liquid and the special quantum critical points. It would be valuable to have a direct comparison between the Ising-Heisenberg and full Heisenberg counterpart models for other classes of the spin chain to build a more complete scenario regarding their relative predictions.

APPENDIX

Here we provide a detailed description of the eigenvectors and eigenvalues of the mixed spin-(1/2, 5/2, 1/2) Ising-Heisenberg branched chain developed for a theoretical mod-

TABLE III. Eigenvectors and eigenenergies (per unit cell) of the model Hamiltonian (1). The probability amplitudes of the quantum states are given in the main text. Here, $\tilde{J}_1 = J_1(\sigma_1^z + \sigma_2^z)$ and $\sigma_1^z = \sigma_2^z = \pm 1/2$.

Eigenenergies	Eigenvectors (basis $|S_{i,1}, S_{i,2}\rangle \otimes |\sigma_i, \sigma_{i+1}\rangle$)
$E_{i1} = -\frac{\tilde{h}}{2} - \frac{5J_2}{4} - \frac{5\tilde{J}_1}{2} - 3h$	$|\psi_{i1}\rangle = |S_{i,1} = \frac{5}{2}, S_{i,2} = \frac{1}{2}\rangle \otimes |\sigma_i, \sigma_{i+1}\rangle$
$E_{i2} = -\frac{\tilde{h}}{2} + \frac{J_2}{4} - 2\tilde{J}_1 - 2h - \frac{1}{2}\sqrt{(2J_2 - \tilde{J}_1)^2 + 5(J_2\Delta)^2}$	$|\psi_{i2}\rangle = a_-|S_{i,1} = \frac{5}{2}, S_{i,2} = -\frac{1}{2}\rangle \otimes |\sigma_i, \sigma_{i+1}\rangle$
	$\quad + a_+|S_{i,1} = \frac{3}{2}, S_{i,2} = \frac{1}{2}\rangle \otimes |\sigma_i, \sigma_{i+1}\rangle$
$E_{i3} = -\frac{\tilde{h}}{2} + \frac{J_2}{4} - 2\tilde{J}_1 - 2h + \frac{1}{2}\sqrt{(2J_2 - \tilde{J}_1)^2 + 5(J_2\Delta)^2}$	$|\psi_{i3}\rangle = a_+|S_{i,1} = \frac{5}{2}, S_{i,2} = -\frac{1}{2}\rangle \otimes |\sigma_i, \sigma_{i+1}\rangle$
	$\quad + a_-|S_{i,1} = \frac{3}{2}, S_{i,2} = \frac{1}{2}\rangle \otimes |\sigma_i, \sigma_{i+1}\rangle$
$E_{i4} = -\frac{\tilde{h}}{2} + \frac{J_2}{4} - \tilde{J}_1 - h - \frac{1}{2}\sqrt{(J_2 - \tilde{J}_1)^2 + 8(J_2\Delta)^2}$	$|\psi_{i4}\rangle = c_-|S_{i,1} = \frac{3}{2}, S_{i,2} = -\frac{1}{2}\rangle \otimes |\sigma_i, \sigma_{i+1}\rangle$
	$\quad + c_+|S_{i,1} = \frac{1}{2}, S_{i,2} = \frac{1}{2}\rangle \otimes |\sigma_i, \sigma_{i+1}\rangle$
$E_{i5} = -\frac{\tilde{h}}{2} + \frac{J_2}{4} - \tilde{J}_1 - h + \frac{1}{2}\sqrt{(J_2 - \tilde{J}_1)^2 + 8(J_2\Delta)^2}$	$|\psi_{i5}\rangle = c_+|S_{i,1} = \frac{3}{2}, S_{i,2} = -\frac{1}{2}\rangle \otimes |\sigma_i, \sigma_{i+1}\rangle$
	$\quad + c_-|S_{i,1} = \frac{1}{2}, S_{i,2} = \frac{1}{2}\rangle \otimes |\sigma_i, \sigma_{i+1}\rangle$
$E_{i6} = -\frac{\tilde{h}}{2} + \frac{J_2}{4} - \frac{1}{2}\sqrt{(\tilde{J}_1)^2 + 9(J_2\Delta)^2}$	$|\psi_{i6}\rangle = e_+|S_{i,1} = \frac{1}{2}, S_{i,2} = -\frac{1}{2}\rangle \otimes |\sigma_i, \sigma_{i+1}\rangle$
	$\quad + e_-|S_{i,1} = -\frac{1}{2}, S_{i,2} = \frac{1}{2}\rangle \otimes |\sigma_i, \sigma_{i+1}\rangle$
$E_{i7} = -\frac{\tilde{h}}{2} + \frac{J_2}{4} + \frac{1}{2}\sqrt{(\tilde{J}_1)^2 + 9(J_2\Delta)^2}$	$|\psi_{i7}\rangle = e_-|S_{i,1} = \frac{1}{2}, S_{i,2} = -\frac{1}{2}\rangle \otimes |\sigma_i, \sigma_{i+1}\rangle$
	$\quad + e_+|S_{i,1} = -\frac{1}{2}, S_{i,2} = \frac{1}{2}\rangle \otimes |\sigma_i, \sigma_{i+1}\rangle$
$E_{i8} = -\frac{\tilde{h}}{2} + \frac{J_2}{4} + \tilde{J}_1 + h - \frac{1}{2}\sqrt{(J_2 + \tilde{J}_1)^2 + 8(J_2\Delta)^2}$	$|\psi_{i8}\rangle = b_+|S_{i,1} = -\frac{1}{2}, S_{i,2} = -\frac{1}{2}\rangle \otimes |\sigma_i, \sigma_{i+1}\rangle$
	$\quad + b_-|S_{i,1} = -\frac{3}{2}, S_{i,2} = \frac{1}{2}\rangle \otimes |\sigma_i, \sigma_{i+1}\rangle$
$E_{i9} = -\frac{\tilde{h}}{2} + \frac{J_2}{4} + \tilde{J}_1 + h + \frac{1}{2}\sqrt{(J_2 + \tilde{J}_1)^2 + 8(J_2\Delta)^2}$	$|\psi_{i9}\rangle = b_-|S_{i,1} = -\frac{1}{2}, S_{i,2} = -\frac{1}{2}\rangle \otimes |\sigma_i, \sigma_{i+1}\rangle$
	$\quad + b_+|S_{i,1} = -\frac{3}{2}, S_{i,2} = \frac{1}{2}\rangle \otimes |\sigma_i, \sigma_{i+1}\rangle$
$E_{i10} = -\frac{\tilde{h}}{2} + \frac{J_2}{4} + 2\tilde{J}_1 + 2h - \frac{1}{2}\sqrt{(2J_2 + \tilde{J}_1)^2 + 5(J_2\Delta)^2}$	$|\psi_{i10}\rangle = d_+|S_{i,1} = -\frac{3}{2}, S_{i,2} = -\frac{1}{2}\rangle \otimes |\sigma_i, \sigma_{i+1}\rangle$
	$\quad + d_-|S_{i,1} = -\frac{5}{2}, S_{i,2} = \frac{1}{2}\rangle \otimes |\sigma_i, \sigma_{i+1}\rangle$
$E_{i11} = -\frac{\tilde{h}}{2} + \frac{J_2}{4} + 2\tilde{J}_1 + 2h + \frac{1}{2}\sqrt{(2J_2 + \tilde{J}_1)^2 + 5(J_2\Delta)^2}$	$|\psi_{i11}\rangle = d_-|S_{i,1} = -\frac{3}{2}, S_{i,2} = -\frac{1}{2}\rangle \otimes |\sigma_i, \sigma_{i+1}\rangle$
	$\quad + d_+|S_{i,1} = -\frac{5}{2}, S_{i,2} = \frac{1}{2}\rangle \otimes |\sigma_i, \sigma_{i+1}\rangle$
$E_{i12} = -\frac{\tilde{h}}{2} - \frac{5J_2}{4} + \frac{5\tilde{J}_1}{2} + 3h$	$|\psi_{i12}\rangle = |S_{i,1} = -\frac{5}{2}, S_{i,2} = -\frac{1}{2}\rangle \otimes |\sigma_i, \sigma_{i+1}\rangle$

eling of the coordination polymer Fe-Mn-Cu. Hamiltonian (1) can be written in the symmetric form as follows:

$$\mathcal{H} = \sum_{i=1}^{N_c} \mathcal{H}_i = \sum_{i=1}^{N_c} \left(-\frac{h}{2}(\sigma_i^z + \sigma_{i+1}^z) + \mathcal{H}_i' \right),$$

where

$$\mathcal{H}_i' = -J_1 S_{i,1}^z (\sigma_i^z + \sigma_{i+1}^z) - \frac{J_2\Delta}{2}(S_{i,1}^+ S_{i,2}^- + S_{i,1}^- S_{i,2}^+)$$
$$- J_2 S_{i,1}^z S_{i,2}^z - h(S_{i,1}^z + S_{i,2}^z). \tag{A1}$$

Here, $S_{i,j}^{\pm}$ are the usual raising and lowering spin-1/2 operators. The Hamiltonian $\mathcal{H}_i'$ can be put in a matrix form in the usual local basis $|S_{i,1}, S_{i,2}\rangle$ representing zth spin components of the Heisenberg dimer corresponding to the magnetic ions Mn^{2+} and Cu^{2+} (the upper index z is left out for easy notation). The matrix representation of Hamiltonian (A1) can be easily diagonalized in decoupled blocks accounting for each magnetization sector. In this form, we have the following matrix representations of the symmetric cell Hamiltonian in all possible magnetization sectors $S_i^t = S_{i,1} + S_{i,2}$.

(a) Magnetization sector $S_i^t = 0$: $|S_{i,1} = 1/2, S_{i,2} = -1/2\rangle$ and $|S_{i,1} = -1/2, S_{i,2} = 1/2\rangle$ subspace,

$$\begin{pmatrix} \frac{J_2}{4} - \frac{\tilde{J}_1}{2} & -\frac{3}{2}J_2\Delta \\ -\frac{3}{2}J_2\Delta & \frac{J_2}{4} + \frac{\tilde{J}_1}{2} \end{pmatrix}, \tag{A2}$$

(b) Magnetization sector $S_i^t = 1$: $|S_{i,1} = 3/2, S_{i,2} = -1/2\rangle$ and $|S_{i,1} = 1/2, S_{i,2} = 1/2\rangle$ subspace,

$$\begin{pmatrix} \frac{3}{4}J_2 - \frac{3}{2}\tilde{J}_1 - h & -J_2\Delta\sqrt{2} \\ -J_2\Delta\sqrt{2} & -\frac{J_2}{4} - \frac{\tilde{J}_1}{2} - h \end{pmatrix}, \tag{A3}$$

(c) Magnetization sector $S_i^t = 2$: $|S_{i,1} = 5/2, S_{i,2} = -1/2\rangle$ and $|S_{i,1} = 3/2, S_{i,2} = 1/2\rangle$ subspace,

$$\begin{pmatrix} -\frac{\tilde{h}}{2} + \frac{5}{4}J_2 - \frac{5}{2}\tilde{J}_1 - 2h & -J_2\Delta\frac{\sqrt{5}}{2} \\ -J_2\Delta\frac{\sqrt{5}}{2} & -\frac{\tilde{h}}{2} - \frac{3}{4}J_2 - \frac{3}{2}\tilde{J}_1 - 2h \end{pmatrix}, \tag{A4}$$

(d) Magnetization sector $S_i^t = 3$: $|S_{i,1} = 5/2, S_{i,2} = 1/2\rangle$ subspace,

$$\left(-\frac{\tilde{h}}{2} - \frac{5}{4}J_2 - \frac{5}{2}\tilde{J}_1 - 3h \right), \tag{A5}$$

(e) Magnetization sector $S_i^t = -1$: $|S_{i,1} = -1/2, S_{i,2} = -1/2\rangle$ and $|S_{i,1} = -3/2, S_{i,2} = 1/2\rangle$ subspace,

$$\begin{pmatrix} -\frac{J_2}{4} + \frac{1}{2}\tilde{J}_1 + h & -J_2\Delta\sqrt{2} \\ -J_2\Delta\sqrt{2} & \frac{3}{4}J_2 + \frac{3}{2}\tilde{J}_1 + h \end{pmatrix}, \tag{A6}$$

(f) Magnetization sector $S_i^t = -2$: $|S_{i,1} = -3/2, S_{i,2} = -1/2\rangle$ and $|S_{i,1} = -5/2, S_{i,2} = 1/2\rangle$ subspace,

$$\begin{pmatrix} -\frac{3}{4}J_2 + \frac{3}{2}\tilde{J}_1 + 2h & -J_2\Delta\frac{\sqrt{5}}{2} \\ -J_2\Delta\frac{\sqrt{5}}{2} & \frac{5}{4}J_2 + \frac{5}{2}\tilde{J}_1 + 2h \end{pmatrix}, \qquad \text{(A7)}$$

(g) Magnetization sector $S_i^t = -3$: $|S_{i,1} = -5/2, S_{i,2} = -1/2\rangle$ subspace,

$$\left(-\frac{\tilde{h}}{2} - \frac{5}{4}J_2 + \frac{5}{2}\tilde{J}_1 + 3h \right), \qquad \text{(A8)}$$

where $\tilde{h} = h(\sigma_1^z + \sigma_2^z)$, $\tilde{J}_1 = J_1(\sigma_1^z + \sigma_2^z)$. The Hamiltonian $\mathcal{H}_i'$ can be exactly diagonalized. The eigenvectors and eigenvalues of the total Hamiltonian can be written in terms of a direct product of the state of each quantum dimer and the states of the neighboring Ising spins. All possible eigenstates and eigenvalues per unit cell are given in Table III.

For the entangled eigenvectors, the coefficients in the quantum superpositions are given by

$$a_\pm^2 = \frac{1}{2}\left[1 \pm \frac{2J_2 - \tilde{J}_1}{\sqrt{(2J_2 - \tilde{J}_1)^2 + 5(J_2\Delta)^2}} \right], \qquad \text{(A9)}$$

$$b_\pm^2 = \frac{1}{2}\left[1 \pm \frac{J_2 + \tilde{J}_1}{\sqrt{(J_2 + \tilde{J}_1)^2 + 8(J_2\Delta)^2}} \right], \qquad \text{(A10)}$$

$$c_\pm^2 = \frac{1}{2}\left[1 \pm \frac{J_2 - \tilde{J}_1}{\sqrt{(J_2 - \tilde{J}_1)^2 + 8(J_2\Delta)^2}} \right], \qquad \text{(A11)}$$

$$d_\pm^2 = \frac{1}{2}\left[1 \pm \frac{2J_2 + \tilde{J}_1}{\sqrt{(2J_2 + \tilde{J}_1)^2 + 5(J_2\Delta)^2}} \right], \qquad \text{(A12)}$$

$$e_\pm^2 = \frac{1}{2}\left[1 \pm \frac{\tilde{J}_1}{\sqrt{\tilde{J}_1^2 + 9(J_2\Delta)^2}} \right], \qquad \text{(A13)}$$

where $\tilde{J}_1 = J_1(\sigma_1^z + \sigma_2^z)$ and $\sigma_1^z = \sigma_2^z = \pm 1/2$.

[1] C. L. M. Pereira, E. F. Pedroso, A. C. Doriguetto, J. A. Ellena, K. Boubekeur, Y. Filali, Y. Journaux, M. A. Novak, and H. O. Stumpf, Dalton Trans. **40**, 746 (2011).

[2] C. Paraschiv, M. Andruh, Y. Journaux, Z. Žak, N. Kyritsakas, and L. Ricard, J. Mater. Chem. **16**, 2660 (2006).

[3] W. R. Entley and G. S. Girolami, Science **268**, 397 (1995).

[4] O. Hatlevik, W. E. Buschmann, J. Zhang, J. L. Manson, and J. S. Miller, Adv. Mater. **11**, 914 (1999).

[5] V. W.-W. Yam, V. K.-M. Au, and S. Y.-L. Leung, Chem. Rev. **115**, 7589 (2015).

[6] X. Feng, L.-F. Ma, L. Liu, L.-Ya. Wang, H.-L. Song, and S.-Y. Xie, Cryst. Growth Des. **13**, 4469 (2013).

[7] C.-D. Wu, C.-Z. Lu, S.-F. Lu, H.-H. Zhuang, and J.-S. Huang, Dalton Trans. **16**, 3192 (2003)

[8] J. S. Seo, D. Whang, H. Lee, S. jun, J. Oh, Y. J. Jeon, and K. Kim, Nature (London) **404**, 982 (2000).

[9] I. Timokhin, C. Pettinari, F. Marchetti, R. Pettinari, F. Condello, S. Galli, E. C. B. A. Alegria, L. M. D. R. S. Martins, and A. J. L. Pombeiro, Cryst. Growth Des. **15**, 2303 (2015).

[10] Y. Nicolet, A. L. de Lacey, X. Vernède, V. M. Fernandez, E. C. Hatchikian, and J. C. Fontecilla-Camps, J. Am. Chem. Soc. **123**, 1596 (2001).

[11] M. Kampa, M.-E. Pandelia, W. Lubitz, M. V. Gastel, and F. Neese, J. Am. Chem. Soc. **135**, 3915 (2013).

[12] N. Magnani, E. Colineau, R. Eloirdi, J.-C. Griveau, R. Caciuffo, S. M. Cornet, I. May, C. A. Sharrad, D. Collison, and R. E. P. Winpenny, Phys. Rev. Lett. **104**, 197202 (2010).

[13] T. C. Stamatatos, K. A. Abboud, W. Wernsdorfer, and G. Christou, Inorg. Chem. **48**, 807 (2009).

[14] R. Clérac, H. Miyasaka, M. Yamashita, and C. Coulon, J. Am. Chem. Soc. **124**, 12837 (2002).

[15] H.-L. Sun, Z.-M. Wang, and S. Gao, Coord. Chem. Rev. **254**, 1081 (2010).

[16] A. H. Morrish, *The Physical Principle of Magnetism* (Wiley, New York, 1966).

[17] L. Bogani, A. Vindigni, R. Sessoli, and D. Gatteschi, J. Mater. Chem. **18**, 4750 (2008).

[18] M. N. Leuenberger and D. Loss, Nature (London) **410**, 789 (2001).

[19] A. Ardavan, O. Rival, J. J. L. Morton, S. J. Blundell, A. M. Tyryshkin, G. A. Timco, and R. E. P. Winpenny, Phys. Rev. Lett. **98**, 057201 (2007).

[20] J.-F. Guo, X.-T. Wang, B.-W. Wang, G.-C. Xu, S. Gao, L. Szeto, W.-T. Wong, W.-Y. Wong, and T.-C. Lau, Chem. Eur. J. **16**, 3524 (2010).

[21] X. Feng, T. D. Harris, and J. R. Long, Chem. Sci. **2**, 1688 (2011).

[22] L. Bogani, L. Cavigli, K. Bernot, R. Sessoli, M. Gurioli, and D. Gatteschi, J. Mater. Chem. **16**, 2587 (2006).

[23] W. Wernsdorfer, R. Clérac, C. Coulon, L. Lecren, and H. Miyasaka, Phys. Rev. Lett. **95**, 237203 (2005).

[24] J. Torrico, M. Rojas, S. M. de Souza, O. Rojas, and N. S. Ananikian, Europhys. Lett. **108**, 50007 (2014).

[25] O. Rojas, M. Rojas, S. M. de Souza, J. Torrico, J. Strečka, and M. L. Lyra, Physica A **486**, 367 (2017).

[26] W. Van den Heuvel and L. F. Chibotaru, Phys. Rev. B **82**, 174436 (2010).

[27] V. Ohanyan and A. Honecker, Phys. Rev. B **86**, 054412 (2012).

[28] Y. Pei, M. Verdaguer, O. Kahn, J. Sletten, and J.-P. Renard, J. Am. Chem. Soc. **108**, 7428 (1986).

[29] X.-Y. Wang, C. Avendaño, and K. R. Dunbar, Chem. Soc. Rev. **40**, 3213 (2011).

[30] L. R. Piquer and E. C. Sañudo, Dalton Trans. **44**, 8771 (2015).

[31] R. Ishikawa, K. Katoh, B. K. Breedlove, and M. Yamashita, Inorg. Chem. **51**, 9123 (2012).

[32] M. Andruh, Chem. Commun. **54**, 3559 (2018).

[33] M. Verdaguer, A. Bleuzen, V. Marvaud, J. Vaissermann, M. Seuleiman, C. Desplanches, A. Scuiller, C. Train, R. Garde, G. Gelly, C. Lomenech, I. Rosenman, P. Veillet, C. Cartier, and F. Villain, Coord. Chem. Rev. **190-192**, 1023 (1999).

[34] D. Deb, S. Duley, S. Radenković, P. Bultinck, P. K. Chattaraj, and M. Bhattacharjee, Phys. Chem. Chem. Phys. **14**, 15579 (2012).

[35] D. Das and M. Bhattacharjee, Eur. J. Inorg. Chem. **2017**, 2828 (2017).

[36] D. Visinescu, J.-P. Sutter, C. R. Pérez, and M. Andruh, Inorg. Chim. Acta **359**, 433 (2006).

[37] M. G. Alexandru, D. Visinescu, S. Shova, M. Andruh, F. Lloret, and M. Julve, Eur. J. Inorg. Chem. **2018**, 360 (2018).

[38] C. N. Verani, T. Weyhermüller, E. Rentschler, E. Bill, and P. Chaudhuri, Chem. Commun. 2475 (1998).

[39] D. Visinescu, M.-G. Alexandru, A. M. Madalan, C. Pichon, C. Duhayon, J.-P. Sutter, and M. Andruh, Dalton Trans. **44**, 16713 (2015).

[40] D. Visinescu, M.-G. Alexandru, A. M. Madalan, I.-R. Jeon, C. Mathonière, R. Clérac, and M. Andruh, Dalton Trans. **45**, 7642 (2016).

[41] L. Sorace, C. Benelli, and D. Gatteschi, Chem. Soc. Rev. **40**, 3092 (2011).

[42] A. M. Madalan, H. W. Roesky, M. Andruh, M. Noltemeyer, and N. Stanica, Chem. Commun. 1638 (2002).

[43] M. Zhu, L. Li, and J.-P. Sutter, Inorg. Chem. Front. **3**, 994 (2016).

[44] A. A. Patrascu, S. Calancea, M. Briganti, S. Soriano, A. M. Madalan, R. A. A. Cassaro, A. Caneschi, F. Totti, M. G. F. Vaz, and M. Andruh, Chem. Commun. **53**, 6504 (2017).

[45] H. Wang, L.-F. Zhang, Z.-H. Ni, W.-F. Zhong, L.-J. Tian, and J. Jiang, Cryst. Growth Des. **10**, 4231 (2010).

[46] F. Souza, M. L. Lyra, J. Strečka, and M. S. S. Pereira, J. Magn. Magn. Mater. **471**, 423 (2019).

[47] K. H. J. Buschow and F. R. de Boer, *Physics of Magnetism and Magnetic Materials* (Kluwer Academic Publishers, New York, 2004).

[48] W. K. Wootters, Phys. Rev. Lett. **80**, 2245 (1998).

[49] S. Hill and W. K. Wootters, Phys. Rev. Lett. **78**, 5022 (1997).

[50] S. Yamamoto, Phys. Rev. B **59**, 1024 (1999).

[51] T. Sakai and S. Yamamoto, J. Magn. Magn. Mater. **226**, 645 (2001).

[52] T. Sakai and K. Okamoto, Phys. Rev. B **65**, 214403 (2002).

[53] A. S. Boyarchenkov, I. G. Bostrem, and A. S. Ovchinnikov, Phys. Rev. B **76**, 224410 (2007).

[54] A. S. F. Tenório, R. R. Montenegro-Filho, and M. D. Coutinho-Filho, J. Phys.: Condens. Matter **23**, 506003 (2011).

[55] M. Oshikawa, M. Yamanaka, and I. Affleck, Phys. Rev. Lett. **78**, 1984 (1997).

[56] T. Sakai and S. Yamamoto, Phys. Rev. B **60**, 4053 (1999).

[57] G.-H. Liu, L.-J. Kong, and J.-Y. Dou, Solid State Commun. **213-214**, 10 (2015).

[58] W. Chen, K. Hida, and B. C. Sanctuary, Phys. Rev. B **67**, 104401 (2003).

[59] A. Kitazawa, J. Phys. A: Math Gen. **30**, L285 (1997).

[60] S. J. Hu, B. Normand, X. Q. Wang, and L. Yu, Phys. Rev. B **84**, 220402(R) (2011).

[61] L. J. De Jongh and A. R. Miedema, Adv. Phys. **23**, 1 (1974).

[62] R. L. Carlin, *Magnetochemistry* (Springer, Berlin, 1986).

[63] O. Kahn, *Molecular Magnetism* (Wiley, New York, 1993).

[64] W. P. Wolf, Braz. J. Phys. **30**, 794 (2000).

[65] L. Amico, R. Fazio, A. Osterloh, and V. Vedral, Rev. Mod. Phys. **80**, 517 (2008).

[66] K. Fegy, D. Luneau, E. Belorizky, M. Novac, J.-L. Tholence, C. Paulsen, T. Ohm, and P. Rey, Inorg. Chem. **37**, 4524 (1998).

[67] J. J. Seiden, Phys. Lett. **44**, 947 (1987).

[68] E. Belorizky and P. Rey, Mol. Phys. **75**, 563 (1992).

[69] S. R. White, Phys. Rev. Lett. **69**, 2863 (1992).

[70] S. R. White, Phys. Rev. B **48**, 10345 (1993).

[71] U. Schollwöck, Rev. Mod. Phys. **77**, 259 (2005).

[72] B. Bauer, L. D. Carr, H. G. Evertz, A. Feiguin, J. Freire, S. Fuchs, L. Gamper, J. Gukelberger, E. Gull, S. Guertler, A. Hehn, R. Igarashi, S. V. Isakov, D. Koop, P. N. Ma, P. Mates, H. Matsuo, O. Parcollet, G. Pawlowski, J. D. Picon *et al.*, J. Stat. Mech. (2011) P05001.

[73] E. Lieb and D. Mattis, J. Math. Phys. **3**, 749 (1962).

[74] T. Giamarchi, *Quantum Physics in One Dimension* (Oxford University Press, New York, 2003).

[75] J. Strečka, Acta Phys. Polon. A **131**, 624 (2017).

[76] J. Strečka and T. Verkholyak, J. Low Temp. Phys. **187**, 712 (2017).

[77] H. W. J. Blöte, J. L. Cardy, and M. P. Nightingale, Phys. Rev. Lett. **56**, 742 (1986).

[78] R. C. Alécio, M. L. Lyra, and J. Strečka, J. Magn. Magn. Mater. **417**, 294 (2016).

[79] K. Karl'ová, J. Strečka, and M. L. Lyra, Phys. Rev. E **100**, 042127 (2019).

[80] L. M. Veríssimo, M. S. S. Pereira, J. Strečka, and M. L. Lyra, Phys. Rev. B **99**, 134408 (2019).

[81] S. Ejima and H. Fehske, Phys. Rev. B **91**, 045121 (2015).

[82] Y.-C. Tzeng, H. Onishi, T. Okubo, and Y.-J. Kao, Phys. Rev. B **96**, 060404(R) (2017).